FULL WAVE LOGGING IN AN IRREGULAR BOREHOLE

by

Michel Bouchon

Laboratoire de Géophysique Interne
IRIGM
Université Joseph Fourier
38041 Grenoble, France

Denis Schmitt[1]

Earth Resources Laboratory
Department of Earth, Atmospheric, and Planetary Sciences
Massachusetts Institute of Technology
Cambridge, MA 02139

ABSTRACT

We present a boundary integral equation formulation for the problem of wave propagation in a borehole of irregular cross-section. The method consists in representing the wave field diffracted at the borehole-rock interface by the radiation from a distribution of surface sources applied along the borehole wall. The wave field in the borehole fluid and in the elastic rock are then expressed using the discrete wavenumber method. The application of the boundary conditions at discretized locations along the borehole wall leads to a linear system of equations. The inversion of this system yields the required source distribution.

We have used the method to investigate the effect of changes in borehole diameter on the pressure wave field inside the borehole. The results show that when the change is smooth, the records obtained ahead of the discontinuity location are not affected by its presence. In the case of a steep variation, however, a significant amount of the Stoneley wave energy is reflected. When the borehole diameter is different at the source and at the receiver levels, the microseismograms obtained are somewhat of an average between the ones that would be recorded in boreholes of constant radius equal to the radius at the source and at the receiver. The presence of small-scale fluctuations in borehole diameter reduces the amplitude of the Stoneley wave and decreases its velocity and the pseudo-Rayleigh wave velocity.

---

[1] Now at Etudes et Productions Schlumberger, 26 Rue de la Cavée, 92142 Clamart, France

INTRODUCTION

Full wave acoustic logs are made up of a large proportion of waves guided along the interface between the borehole fluid and the elastic rock. The presence of discontinuities in this wave guide such as the crossing of bed boundaries and fractures strongly affects the propagation of the waves (Paillet, 1980; Arditty et al., 1984; Paternoster, 1985; Hardin et al., 1987). Stephen et al. (1985) have used finite-difference schemes to numerically model such configurations. They studied more particularly the presence of washouts and horizontal fissures and showed that their presence greatly affects Stoneley wave amplitude and waveform.

In the present paper we investigate the effect of changes in borehole radius on the pressure wave field inside the borehole. We use the discrete wavenumber formulation applied in cylindrical geometry (Cheng and Toksöz; 1981; Cheng et al., 1982; Tubman et al., 1984; Schmitt and Bouchon, 1985; Schmitt et al., 1988) and combine it with a boundary integral equation approach (Bouchon, 1985; Campillo and Bouchon, 1985).

DESCRIPTION OF THE METHOD

The configuration studied consists of a fluid-filled borehole surrounded by an homogeneous elastic formation. The borehole radius is allowed to vary vertically but the geometry of the well is symmetric with respect to the borehole axis. The source is a dilatational point located at the center of the borehole. The receivers may be placed anywhere.

In a cylindrical coordinate system (r, θ, z), centered along the borehole axis, the steady-state radiation from a source located at (r_0, θ_0, z_0) may be expressed as (e.g., Gradshteyn and Rhyzhik, 1965):

$$\frac{e^{-i\omega R/\alpha}}{R} = \frac{1}{\pi} \int_{-\infty}^{\infty} K_0 \left[\nu(r^2 + r_0^2 - 2rr_0 \cos(\theta - \theta_0))^{\frac{1}{2}}\right] e^{ik(z-z_0)} dk \qquad (1)$$

with $\nu = \left[k^2 - \frac{\omega^2}{\alpha^2}\right]^{\frac{1}{2}}$, and where ω denotes the angular frequency, α is the compressional wave velocity, R is the distance between source and observation point, K_0 denotes the modified Bessel function of the second kind of the zeroth order, and the $e^{i\omega t}$ time dependence is understood.

Using the Bessel function addition theorem (Watson, 1922) one obtains:

$$\frac{e^{-i\omega R/\alpha}}{R} = \frac{1}{\pi} \int_{-\infty}^{\infty} \sum_{n=0}^{\infty} \xi_n \cos n(\theta - \theta_0) I_n(\nu r_0) K_n(\nu r) e^{ik(z-z_0)} \qquad \text{for } r \geq r_0$$

and

$$\frac{e^{-i\omega R/\alpha}}{R} = \frac{1}{\pi}\int_{-\infty}^{\infty}\sum_{n=0}^{\infty}\xi_n \cos n(\theta-\theta_0)K_n(\nu r_0)I_n(\nu r)e^{ik(z-z_0)}dk \qquad \text{for } r \le r_0 \tag{2}$$

with $\xi_n = 1$ for $n = 0$, and $\xi_n = 2$ for $n \neq 0$, where I_n and K_n denote the modified Bessel functions of order n.

For a source located in the middle of the borehole at depth z_0, Eq. (2) becomes:

$$\phi = \frac{e^{-i\omega R/\alpha}}{R} = \frac{1}{\pi}\int_{-\infty}^{\infty} K_0(\nu r)e^{ik(z-z_0)}dk\ . \tag{3}$$

We now introduce a periodicity in the source-medium configuration along the z-axis. This replaces the integral in Eq. (3) by a discrete summation (Bouchon and Aki, 1977). Eq. (3) then becomes (Cheng and Toksöz, 1981):

$$\phi = \frac{2}{L}\sum_{m=-\infty}^{\infty} K_0(\nu_m r)e^{ik_m(z-z_0)} \tag{4}$$

with $k_m = 2\pi m/L$, $\nu_m = \left(k_m^2 - \frac{\omega^2}{\alpha^2}\right)^{\frac{1}{2}}$, $m = 0, \pm 1, \ldots$ and where L is the periodicity length.

We next discretize the borehole wall at equal interval Δz along the vertical axis. We choose Δz such that:

$$L = N\Delta z \text{ where } N \text{ is an odd integer,} \tag{5}$$

and we evaluate the resulting displacement and stress at the discretized points in the direction normal to the borehole wall. We obtain, denoting by $n_{r,j}$ and $n_{z,j}$ the radial and vertical components of the normal to the interface at depth z_j:

$$\begin{aligned} u_{n,j} &= u_{r,j}n_{r,j} + u_{z,j}n_{z,j} \\ t_{n,j} &= \sigma_{rr,j} \end{aligned} \tag{6}$$

with

$$\begin{aligned} u_{r,j} &= -\frac{2}{L}\sum_{m=-\infty}^{\infty}\nu_m K_1(\nu_m r_j)e^{ik_m(z_j-z_0)} \\ u_{z,j} &= \frac{2i}{L}\sum_{m=-\infty}^{\infty} k_m K_0(\nu_m r_j)e^{ik_m(z_j-z_0)} \\ \sigma_{rr,j} &= -\frac{2}{L}\rho\omega^2\sum_{m=-\infty}^{\infty} K_0(\nu_m r_j)e^{ik_m(z_j-z_0)} \end{aligned} \tag{7}$$

where ρ denotes the density.

Applying Huygens' principle, we represent the wavefield diffracted at the borehole wall by the superposition of the radiation from sources distributed along the surface of the borehole. The acoustic wavefield reflected inside the borehole is represented by dilatational sources, while the elastic field transmitted into the surrounding rock is described by forces acting in directions normal and tangential to the borehole wall. Because of the z-discretization that we have introduced, these three sets of surface sources are reduced to three distributions of circular sources.

The radiation from a circular dilatational source of radius r_i located at depth z_i is:

$$\phi = \int_0^{2\pi} \frac{e^{-i\omega R/\alpha}}{R} d\theta_i \ , \quad \text{with } R = [(z-z_i)^2 + (r_i\cos\theta_i - r\cos\theta)^2 + (r_i\sin\theta_i - r\sin\theta)^2]^{\frac{1}{2}}$$

that is, using Eq. (2):

$$\phi = 2\int_{-\infty}^{\infty} I_0(\nu r_i)K_0(\nu r)e^{ik(z-z_i)}dk \qquad \text{for } r \geq r_i$$

$$\phi = 2\int_{-\infty}^{\infty} K_0(\nu r_i)I_0(\nu r)e^{ik(z-z_i)}dk \qquad \text{for } r \leq r_i \ . \tag{8}$$

The periodicity in z replaces the integrals in Eqs. (8) by discrete summations, that is:

$$\phi = \frac{4\pi}{L}\sum_{m=-\infty}^{\infty} I_0(\nu_m r_i)K_0(\nu_m r)e^{ik_m(z-z_i)} \quad \text{for } r \geq r_i$$

$$\phi = \frac{4\pi}{L}\sum_{m=-\infty}^{\infty} K_0(\nu_m r_i)I_0(\nu_m r)e^{ik_m(z-z_i)} \quad \text{for } z \leq r_i \ . \tag{9}$$

The radiation from the whole distribution of dilatational sources representing the diffracted wave field inside the borehole is thus:

$$\phi = \frac{4\pi}{L}\sum_{i=0}^{N} Q_i \sum_{m=-\infty}^{\infty} G_\alpha(r_i, r)e^{ik_m(z-z_i)} \tag{10}$$

$$\text{with} \quad G_\alpha(r_i, r) = I_0(\nu_m r_i)K_0(\nu_m r) \quad \text{for } r \geq r_i$$

$$G_\alpha(r_i, r) = K_0(\nu_m r_i)I_0(\nu_m r) \quad \text{for } r \leq r_i$$

and where Q_i is the intensity of the circular source i of radius r_i applied at depth $z_i = i\Delta z$.

However, the discretization in z implies a periodicity in wavenumber space (Bouchon, 1985; Campillo and Bouchon, 1986) so that Eq. (10) becomes:

$$\phi = \frac{4\pi}{L} \sum_{i=0}^{N} Q_i \sum_{m=-M}^{M} G_\alpha(r_i, r) e^{ik_m(z-z_i)} \tag{11}$$

where M is such that $N = 2M + 1$.

The displacement and stress components at the location (r_j, z_j) of the borehole wall may thus be written:

$$\begin{aligned} u_{r,j} &= -\frac{4\pi}{L} \sum_{i=0}^{N} Q_i \sum_{m=-M}^{M} \nu_m G_{\alpha,1}(r_i, r_j) e^{ik_m(z_j-z_i)} \\ u_{z,j} &= \frac{4\pi i}{L} \sum_{i=0}^{N} Q_i \sum_{m=-M}^{M} k_m G_\alpha(r_i, r_j) e^{ik_m(z_j-z_i)} \\ \sigma_{rr,j} &= -\frac{4\pi}{L} \rho\omega^2 \sum_{i=0}^{N} Q_i \sum_{m=-M}^{M} G_\alpha(r_i, r_j) e^{ik_m(z_j-z_i)} \end{aligned} \tag{12}$$

$$\begin{aligned} \text{with} \quad G_{\alpha,1}(r_i, r_j) &= I_0(\nu_m r_i) K_1(\nu_m r_j) \quad \text{for } r_j \geq r_i \\ G_{\alpha,1}(r_i, r_j) &= -K_0(\nu_m r_i) I_1(\nu_m r_j) \quad \text{for } r_j \leq r_i \,. \end{aligned}$$

From these expressions, the displacement and stress normal to the borehole wall are readily obtained using Eq. (6).

Similarly, we must now derive the expressions of the diffracted wavefield in the elastic formation. The displacement field generated by a steady-state vertical point force of strength F may be written in the form (e.g., Harkrider, 1964):

$$\begin{aligned} u_r &= \frac{F}{4\pi\rho\omega^2} \frac{\partial^2}{\partial r \partial z} \left(\frac{e^{-i\omega R/\beta} - e^{-i\omega R/\alpha}}{R} \right) \\ u_z &= \frac{F}{4\pi\rho\omega^2} \left[\frac{\partial^2}{\partial z^2} \left(\frac{e^{-i\omega R/\beta} - e^{-i\omega R/\alpha}}{R} \right) + \frac{\omega^2}{\beta^2} \frac{e^{-i\omega R/\beta}}{R} \right] \end{aligned} \tag{13}$$

where β denotes the shear wave velocity. In the case of a horizontal force acting in the θ_0 direction, one gets (e.g., Harkrider, 1964; Kurkjian, 1986):

$$u_r = \frac{F}{4\pi\rho\omega^2}\cos(\theta-\theta_0)\left[\frac{\partial^2}{\partial r^2}\left(\frac{e^{-i\omega R/\beta}-e^{-i\omega R/\alpha}}{R}\right)+\frac{\omega^2}{\beta^2}\frac{e^{-i\omega R/\beta}}{R}\right]$$

$$u_z = \frac{F}{4\pi\rho\omega^2}\cos(\theta-\theta_0)\frac{\partial^2}{\partial r\partial z}\left(\frac{e^{-i\omega R/\beta}-e^{-i\omega R/\alpha}}{R}\right) . \qquad (14)$$

Using Eq. (2) in the relations (13) and (14) and integrating the point force solution over a circle of radius r_i, one obtains for the displacement field radiated by a circular vertical force of strength $F_{z,i}$ applied at (r_i, z_i) the expressions:

$$u_r = \frac{iF_{z,i}}{L\rho\omega^2}\sum_{m=-\infty}^{\infty} k_m(\nu_m G_{\alpha,1}(r_i,r)-\gamma_m G_{\beta,1}(r_i,r))\, e^{ik_m(z-z_i)}$$

$$u_z = \frac{F_{z,i}}{L\rho\omega^2}\sum_{m=-\infty}^{\infty} [k_m^2 G_\alpha(r_i,r)-\gamma_m^2 G_\beta(r_i,r)]\, e^{ik_m(z-z_i)} \qquad (15)$$

with, for $r \geq r_i$: $G_\beta(r_i,r) = I_0(\gamma_m r_i)K_0(\gamma_m r)$

$$G_{\beta,1}(r_i,r) = I_0(\gamma_m r_i)K_1(\gamma_m r)$$

and for $r \leq r_i$: $G_\beta(r_i,r) = K_0(\gamma_m r_i)I_0(\gamma_m r)$

$$G_{\beta,1}(r_i,r) = -K_0(\gamma_m r_i)I_1(\gamma_m r)$$

and where $\gamma_m = \left(k_m^2-\frac{\omega^2}{\beta^2}\right)^{\frac{1}{2}}$.

The corresponding expressions for a circular radial force are:

$$u_r = \frac{F_{r,i}}{L\rho\omega^2}\sum_{m=-\infty}^{\infty}\left[\frac{\partial^2}{\partial r^2}(G_{\beta,2}(r_i,r)-G_{\alpha,2}(r_i,r))+\frac{\omega^2}{\beta^2}G_{\beta,2}(r_i,r)\right] e^{ik_m(z-z_i)}$$

$$u_z = \frac{iF_{r,i}}{L\rho\omega^2}\sum_{m=-\infty}^{\infty} k_m\frac{\partial}{\partial r}(G_{\beta,2}(r_i,r)-G_{\alpha,2}(r_i,r))\, e^{ik_m(z-z_i)} \qquad (16)$$

with $G_{\alpha,2}(r_i,r) = I_1(\nu_m r_i)K_1(\nu_m r)$ for $r \geq r_i$

$$G_{\alpha,2}(r_i,r) = K_1(\nu_m r_i)I_1(\nu_m r) \text{ for } r \leq r_i .$$

The expressions of the diffracted displacement field at location (r_j, z_J) of the borehole wall are thus:

$$
\begin{aligned}
u_{r,j} &= \frac{i}{L\rho\omega^2}\sum_{i=0}^{N} F_{z,i} \sum_{m=-M}^{M} k_m(\nu_m G_{\alpha,1}(r_i,r_j) - \gamma_m G_{\beta,1}(r_i,r_j))e^{ik_m(z_j-z_j)} \\
&\quad + \frac{1}{L\rho\omega^2}\sum_{i=0}^{N} F_{r,i} \sum_{m=-m}^{M} \left[\frac{\partial^2}{\partial r^2}(G_{\beta,2}(r_i,r_j) - G_{\alpha,a}(r_i,r_j)) + \frac{\omega^2}{\beta^2}G_{\beta,2}(r_i,r_j)\right] e^{ik_m(z_j-z_i)} \\
u_{z,j} &= \frac{1}{L\rho\omega^2}\sum_{i=0}^{N} F_{z,i} \sum_{m=-M}^{M} [k_m^2 G_\alpha(r_i,r_j) - \gamma_m^2 G_\beta(r_i,r_j))^{ik_m(z_j-z_j)} \qquad (17) \\
&\quad + \frac{i}{L\rho\omega^2}\sum i = 0^N F_{r,i} \sum_{m=-M}^{M} k_m \frac{\partial}{\partial r}(G_{\beta,2}(r_i,r_j) - G_{\alpha,2}(r_i,r_j))e^{ik_m(z_j-z)j)} .
\end{aligned}
$$

From these expressions, the components of the displacement and stress normal n to the borehole wall and of the stress tangential t to it are readily obtained through the relations:

$$
\begin{aligned}
u_{n,j} &= u_{r,j}n_{r,j} + u_{z,j}n_{z,j} \\
t_{n,j} &= \sigma_{rr,j}n_{r,j}^2 + \sigma_{zz,j}n_{z,j}^2 + 2\sigma_{rz,j}n_{r,j}n_{z,j} \\
t_{t,j} &= -\sigma_{rr,j}n_{r,j}n_{z,j} + \sigma_{zz,j}n_{r,j}n_{z,j} + \sigma_{rz,j}(n_{r,j}^2 - n_{z,j}^2) \qquad (18)
\end{aligned}
$$

with

$$
\begin{aligned}
\sigma_{rr} &= \lambda\left(\frac{\partial u_r}{\partial r} + \frac{u_r}{r} + \frac{\partial u_z}{\partial z}\right) + 2\mu\frac{\partial u_r}{\partial r} \\
\sigma_{zz} &= \lambda\left(\frac{\partial u_r}{\partial r} + \frac{u_r}{r} + \frac{\partial u_z}{\partial z}\right) + 2\mu\frac{\partial u_z}{\partial z} \\
\sigma_{rz} &= \mu\left(\frac{\partial u_r}{\partial z} + \frac{\partial u_z}{\partial r}\right)
\end{aligned}
$$

and where λ and μ are the Lamé coefficients.

The boundary conditions at the borehole wall require that the tangential stress is null and that the normal displacement and the normal stress are continuous. Therefore, using the expressions that we have derived above for these observables and matching the boundary conditions at the N discretized depths yield a linear system of equations where the unknowns are the source strengths Q_i, $F_{z,i}$, and $F_{r,i}$. The inversion of the system gives the surface source distribution which describes the scattered wavefield anywhere in the medium.

The calculation is carried out for equally-spaced frequencies spanning the interval [0 Hz, $f_{\max}$] where $f_{\max}$ is the highest frequency desired. The periodicity L in the source medium configuration is chosen such that no disturbance from the neighboring

sources or from the neighboring diffractors arrives at the receivers in the time window of interest. Aliasing of the seismograms is avoided by giving to the frequency an imaginary part equal to $\omega_i = -\pi/T$ where T denotes the length of the time window. The effect of this imaginary part is later removed from the time domain solution.

RESULTS

Borehole of Smoothly Varying Radius

The first borehole geometry that we consider is depicted in Figure 1a. The borehole radius varies smoothly from 12cm to 7cm. The fluid wave velocity is 1500m/s and its density is 1g/cm^3. The formation elastic parameters chosen to represent those of a limestone rock are $\alpha = 3600$m/s, $\beta = 2300$ m/s, and $\rho = 2.5$g/cm^3. The source is located in the widest part of the borehole and emits a Ricker pressure pulse with a peak frequency of 5kHz. The microseismograms recorded at an array of 30 receivers located along the borehole axis at distances ranging from 10cm to 3m from the source are displayed in Figure 2. The calculation is done from 0 to 21kHz. The periodicity length L is equal to 9m. The value of N is equal to 61 at low frequencies and subsequently increases according to the criterion $\Delta x = \gamma_{\text{fluid}}/3$ where γ_{fluid} denotes the wavelength in the borehole fluid.

The results presented in Figure 2 may be compared with those obtained for boreholes of constant radius equal to 12cm (Figure 3) and 7cm (Figure 4). The comparison shows that the signals recorded at locations ahead of the radius change are not visibly affected by it. As the calculation depicted in Figure 3 was performed using reflection and transmission coefficients at the borehole wall, the good agreement between the results of Figures 2 and 3 at the first receivers shows the validity of the boundary integral formulation.

At the receivers located beyond the change in borehole diameter, the microseismogram characteristics are somewhat of an average between those corresponding to radii of 12 and 7cm. The pseudo-Rayleigh wave excitation is higher than in the case of the 7cm radius borehole, but not as high as for the larger borehole (Figure 5). The Stoneley wave amplitude is larger than for the 12cm radius borehole, but is only half of what is expected for a constant 7cm radius. Although small, the level of P wave excitation also lies between the levels obtained for boreholes of 12 and 7cm. Using the reciprocity principle, an exchange of position between the source and the receiver located 2m from it would result in the same signal. The above observations thus hold for a configuration where the source is located in the narrowest part of the well and receivers are spread a few meters away, in the widest part of the borehole.

Effect of Small-Scale Borehole Irregularities

In order to investigate the effect of small-scale borehole irregularities on the propagating wave field, we consider the geometry depicted in Figure 1b. The borehole radius varies continuously between 11 and 13cm. The variation occurs smoothly over a periodicity length of 50cm. The comparison of the results obtained with those corresponding to the case of a constant 12cm radius (the average radius of the irregular well) is displayed in Figure 6. The peak frequency of the source is 4kHz. The other parameters are the same as the ones used in the previous applications.

The two major features of the results are the slight amplitude reduction of the Stoneley wave and its increased delay time in the presence of radius fluctuations.

Effect of Steep Radius Variation

We now consider the borehole geometry depicted in Figure 1c. As in the configuration of Figure 1a studied earlier, the radius decreases from a value of 12cm near the source to 7cm. The change, however, now takes place over a 10cm depth interval and occurs at a distance of 1m from the source. The other parameters are unchanged. The calculated microseismograms are presented in Figure 7. They correspond to a peak source spectrum of 3.5kHz chosen to emphasize the Stoneley wave. The steep change in the borehole cross-section gives rise to a reflected Stoneley wave. The comparison with the case of a smooth diameter change (Figure 1a) is displayed in Figure 8. It shows a decrease in amplitude of the Stoneley wave transmitted across the steep radial discontinuity.

The perfect agreement between the signals recorded at close range for the two geometries before the arrival of the reflected waves shows the good stability of the method. Indeed, different values of the periodicity length ($L = 7$m and $L = 9$m) and of the number of discretized depths at low frequencies ($N = 181$ and $N = 61$) were used for the two calculations. The smaller depth sampling relied upon at low frequency in the presence of a steep discontinuity was designed to provide a finer image of the borehole wall in this case.

CONCLUSION

We have formulated the boundary integration equation-discrete wavenumber representation method in the case of borehole wave propagation. We have used the method to investigate the effect of variations in the borehole cross-section on the pressure field inside the borehole. The results obtained show that a smooth variation in borehole

radius does not affect the records obtained ahead of the discontinuity location, but that the presence of a steep cross-section discontinuity reflects a significant amount of the Stoneley wave energy. When the borehole diameter is different at the source and at the receiver levels, the characteristics of the microseismograms are somewhat of an average between the characteristics that would be obtained for boreholes of constant radii equal to the radius at the source and to the radius at the receiver. Finally, the presence of small-scale irregularities of the borehole wall reduces the amplitude of the Stoneley wave and decreases its velocity and the velocity of the pseudo-Rayleigh wave.

ACKNOWLEDGEMENTS

This work was supported by the Full Waveform Acoustic Logging Consortium at M.I.T. and by the Société Nationale Elf Aquitaine (Production).

REFERENCES

Arditty, P.C., Arens, G., and Staron, P., Improvement of formations properties evaluation through the processing and interpretation results of the EVA tool recordings, *54th Ann. Int. Mtg. Soc. Explor. Geophys.*, Atlanta, Georgia, 1984.

Bouchon, M., A simple, complete numerical solution to the problem of diffraction of SH waves by an irregular interface, *J. Acoust. Soc. Am., 77,* 1–5, 1985.

Bouchon, M., and Aki, K., Discrete wavenumber representation of seismic source wave fields, *Bull. Seis. Soc. Am., 67,* 259–277, 1977.

Campillo, M., and Bouchon, M., Synthetic SH-seismograms in a laterally varying medium by the discrete wavenumber method, *Geophys. J. Roy. Astr. Soc., 83,* 307–317, 1985.

Cheng, C.H., and Toksöz, M.N., Elastic wave propagation in a fluid filled borehole and synthetic acoustic logs, *Geophysics, 46,* 1042–1053, 1981.

Cheng, C.H., Toksöz, M.N., and Willis, M.E., Determination of in situ attenuation from full waveform acoustic logs, *J. Geophys. Res., 87,* 5477–5484, 1982.

Gradshteyn, I.S., and Rhyzhik, I.M., *Table of Integrals, Series and Products,* Academic Press, New York, 1965.

Hardin, E.G., Cheng, C.H., Paillet, F.L., and Mendelson, J.D., Fracture characterization by means of attenuation and generation of tube waves in fractured crystalline rock at Mirror Lake, New Hampshire, *J. Geophys. Res., 92,* 7989–8006, 1987.

Harkrider, D.G., Surface waves in multilayered elastic media, Part I. Rayleigh and Love waves from buried sources in multilayered half-space, *Bull. Seis. Soc. Am., 54,* 627–680, 1964.

Kurkjian, A.L., Theoretical far-field radiation from low-frequency horizontal acoustic point force in a vertical borehole, *Geophysics, 51,* 930–939, 1986.

Paillet, F.L., Acoustic propagation in the vicinity of fractures which intersect a fluid filled borehole, *Trans. SPWLA 21st Ann. Logging Symp.*, Paper DD, 1980.

Paternoster, B., Effects of layer boundaries on full waveform acoustic logs, M.S. Thesis, Massachusetts Institute of Technology, Cambridge, Massachusetts, 1985.

Schmitt, D.P., and Bouchon, M., Full wave acoustic logging: synthetic microseismograms and frequency wavenumber analysis, *Geophysics, 50,* 1756–1778, 1985.

Schmitt, D.P., Bouchon, M., and Bonnet, G., Full wave synthetic logs in radially semi-

infinite saturated porous media, *Geophysics,* in press, 1988.

Stephen, R.A., Pardo-Casas, F., and Cheng, C.H., Finite-difference synthetic acoustic logs, *Geophysics, 50,* 1588-1609, 1985.

Tubman, K.M., Cheng, C.H., and Toksöz, M.N., Synthetic full-waveform acoustic logs in cased boreholes, *Geophysics, 49,* 1051–1059, 1984.

Watson, G.N., *A Treatise on the Theory of Bessel Functions,* Cambridge University Press, Cambridge, 1922.

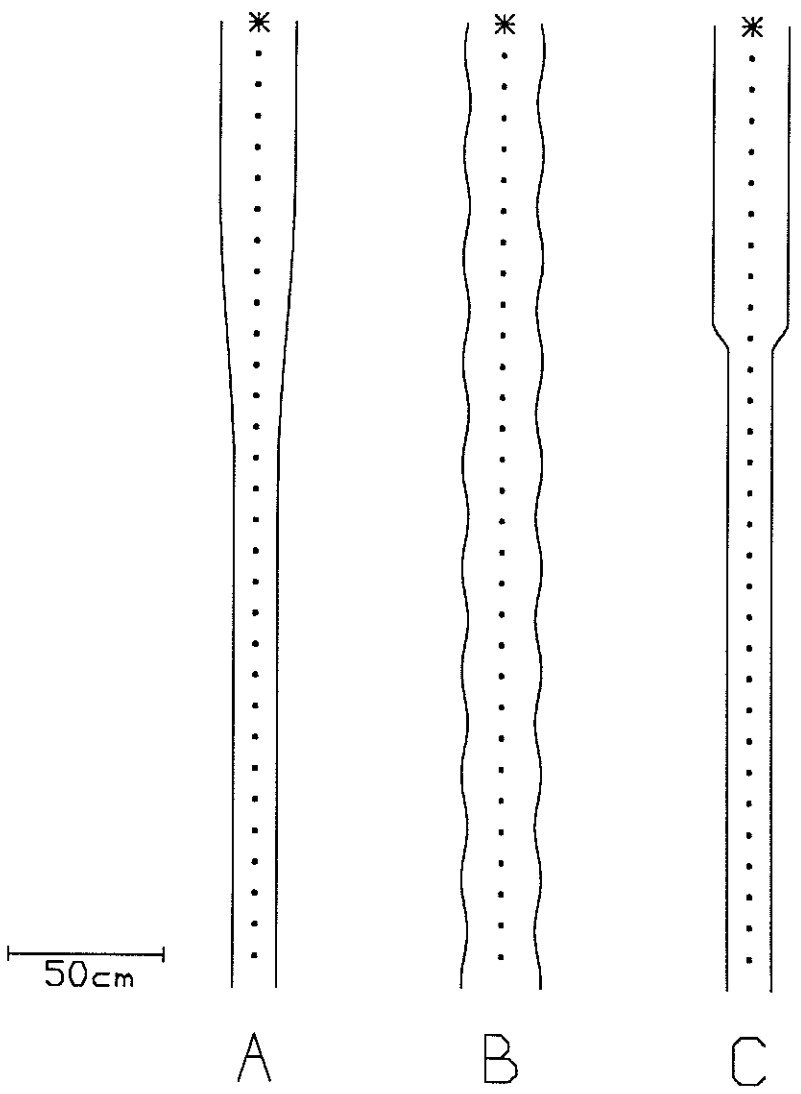

Figure 1: Borehole geometries and source-receivers configurations studied. In Figure 1a the radius changes sinusoidally from 12cm at an axial distance of 50cm from the source to a value of 7cm at a distance of 1.50cm. In Figure 1c the same change occurs between distances of 95cm and 1.05m. In Figure 1b the radius fluctuates sinusoidally between 11cm and 13cm, with a wavelength of fluctuation of 50cm.

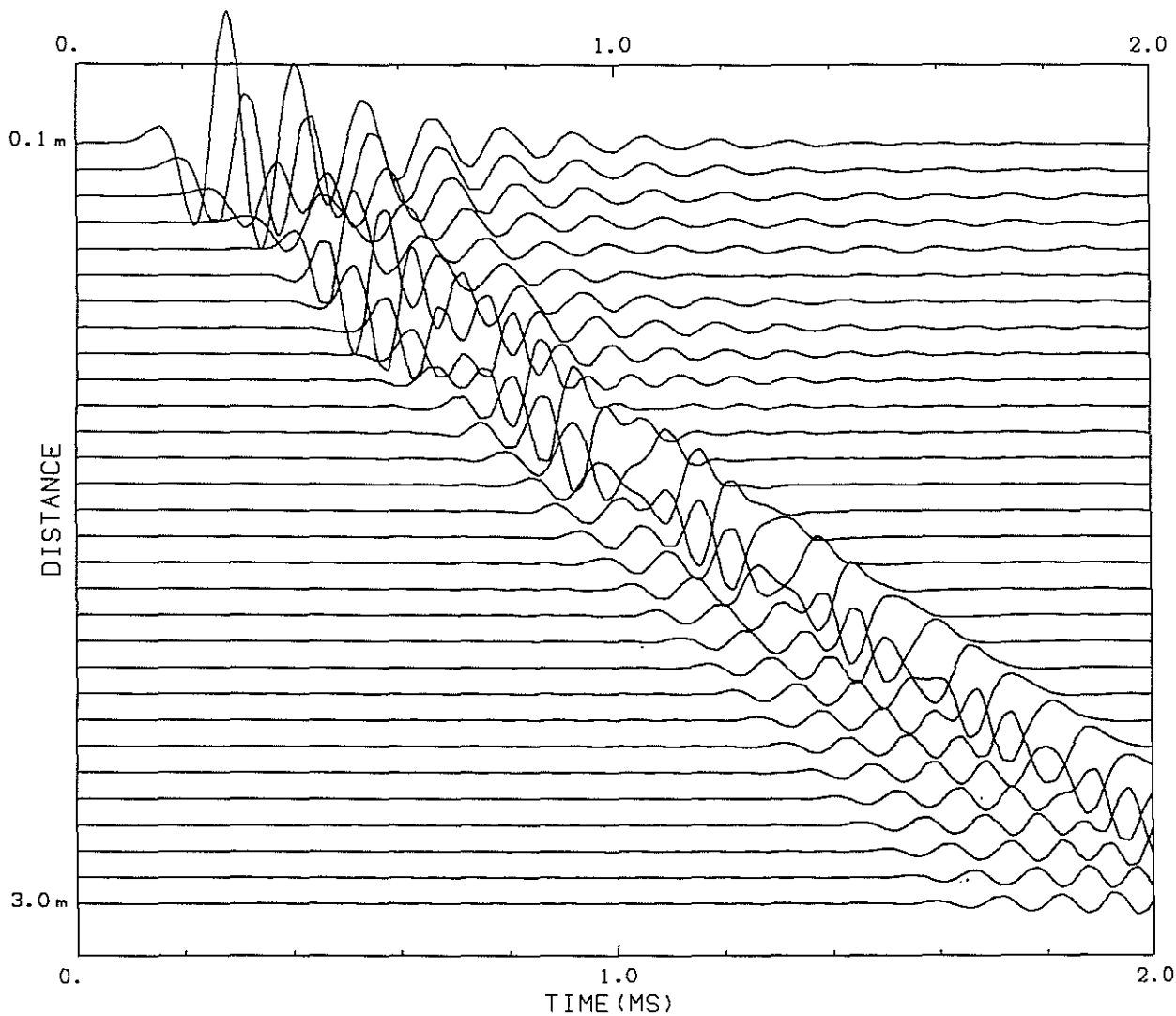

Figure 2: Synthetic acoustic logs obtained for the configuration of Figure 1a. The source is a Ricker wavelet of 5kHz peak frequency. The origin time is 0.1ms before the time of maximum pressure at the source. The direct water pulse is not included.

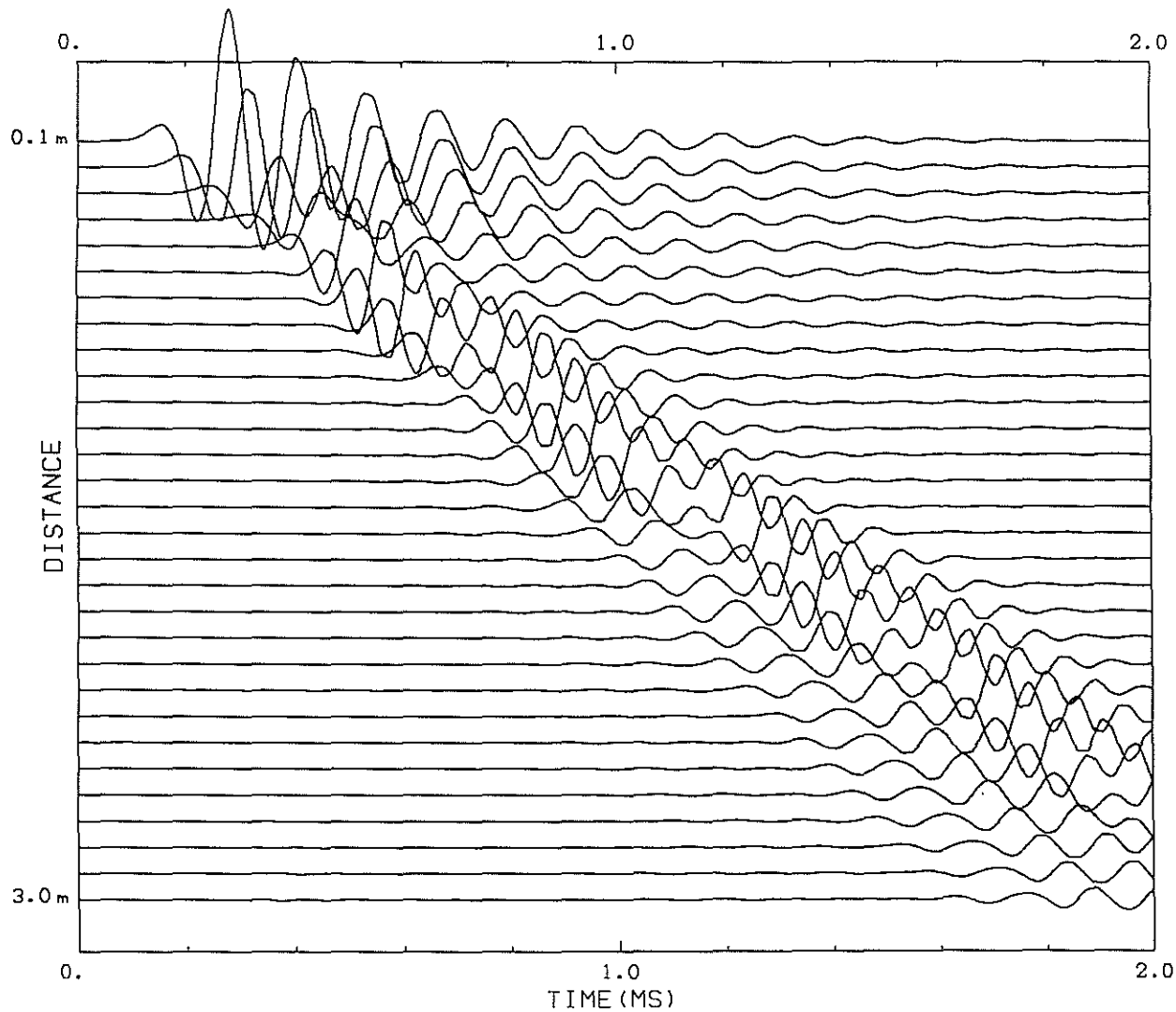

Figure 3: Same as Figure 2 for a borehole of constant radius equal to 12cm.

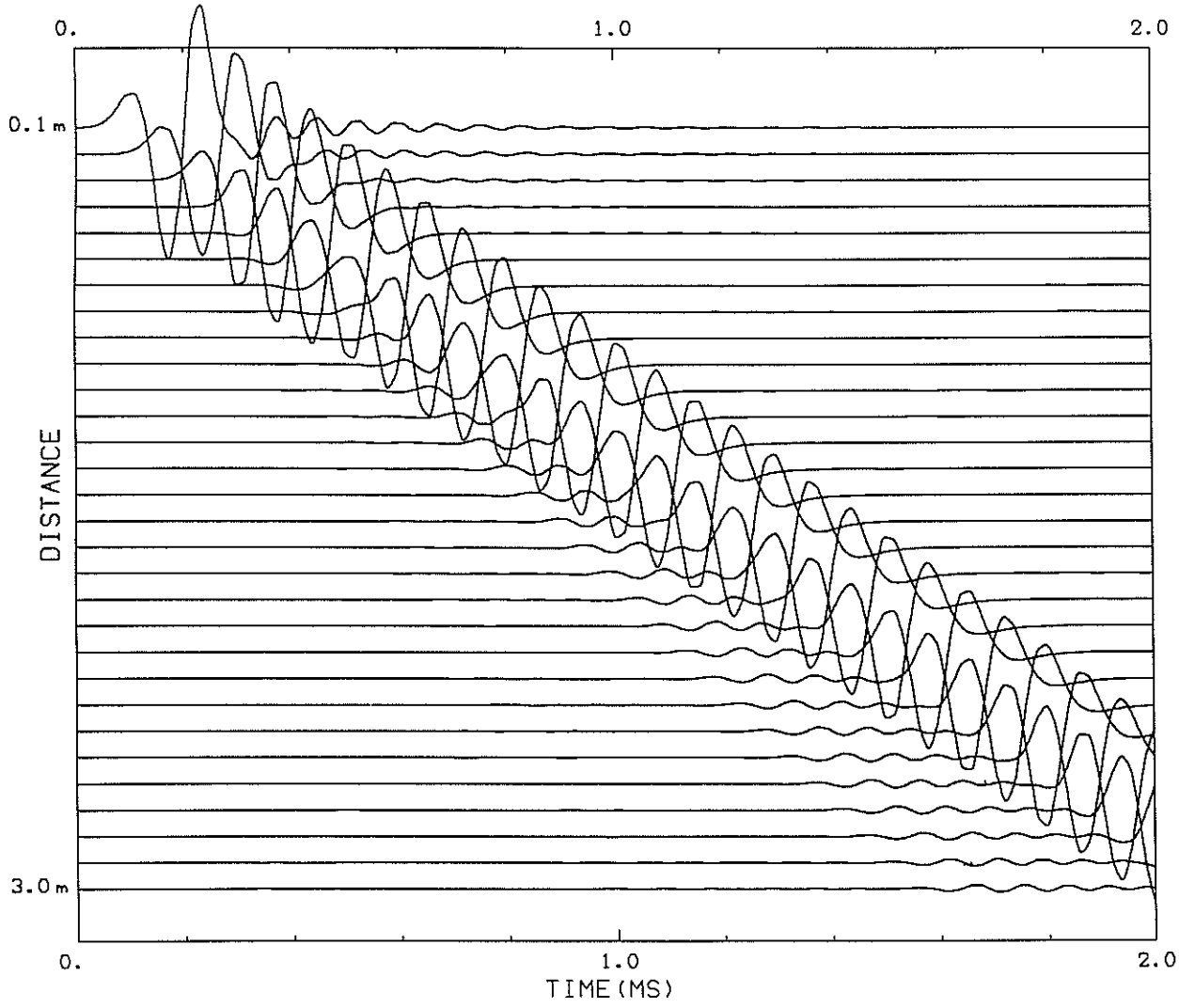

Figure 4: Same as Figure 2 for a borehole of constant radius equal to 7cm.

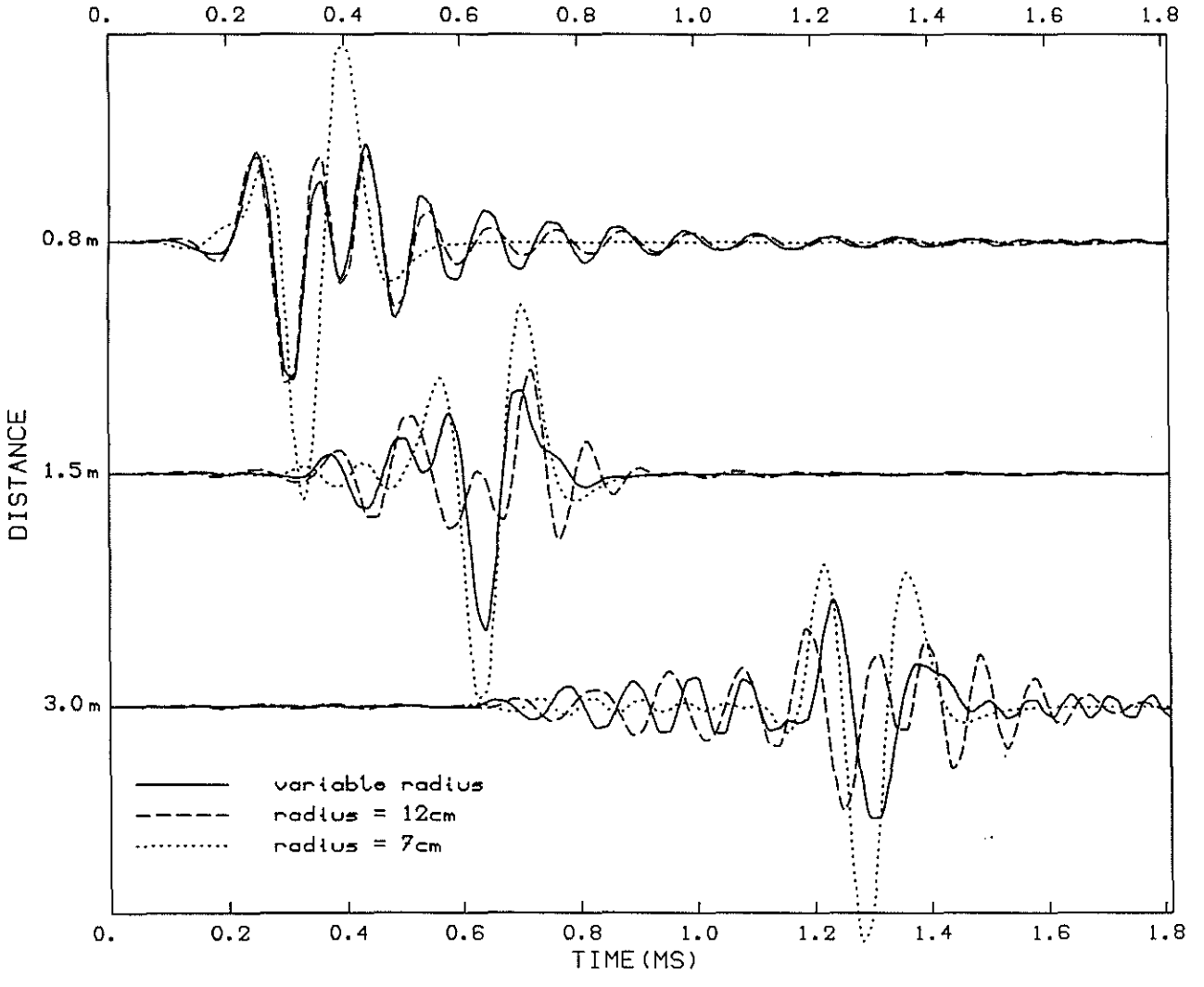

Figure 5: Comparison of the microseismograms obtained for a borehole radius varying between 12 and 7cm (Figure 1a) with those corresponding to constant borehole radii of 12cm and 7cm. The source is a Ricker wavelet of 5kHz peak frequency. The origin of the time scale is the time of maximum pressure at the source minus a delay time which is equal to the axial distance divided by the P-wave velocity in the formation.

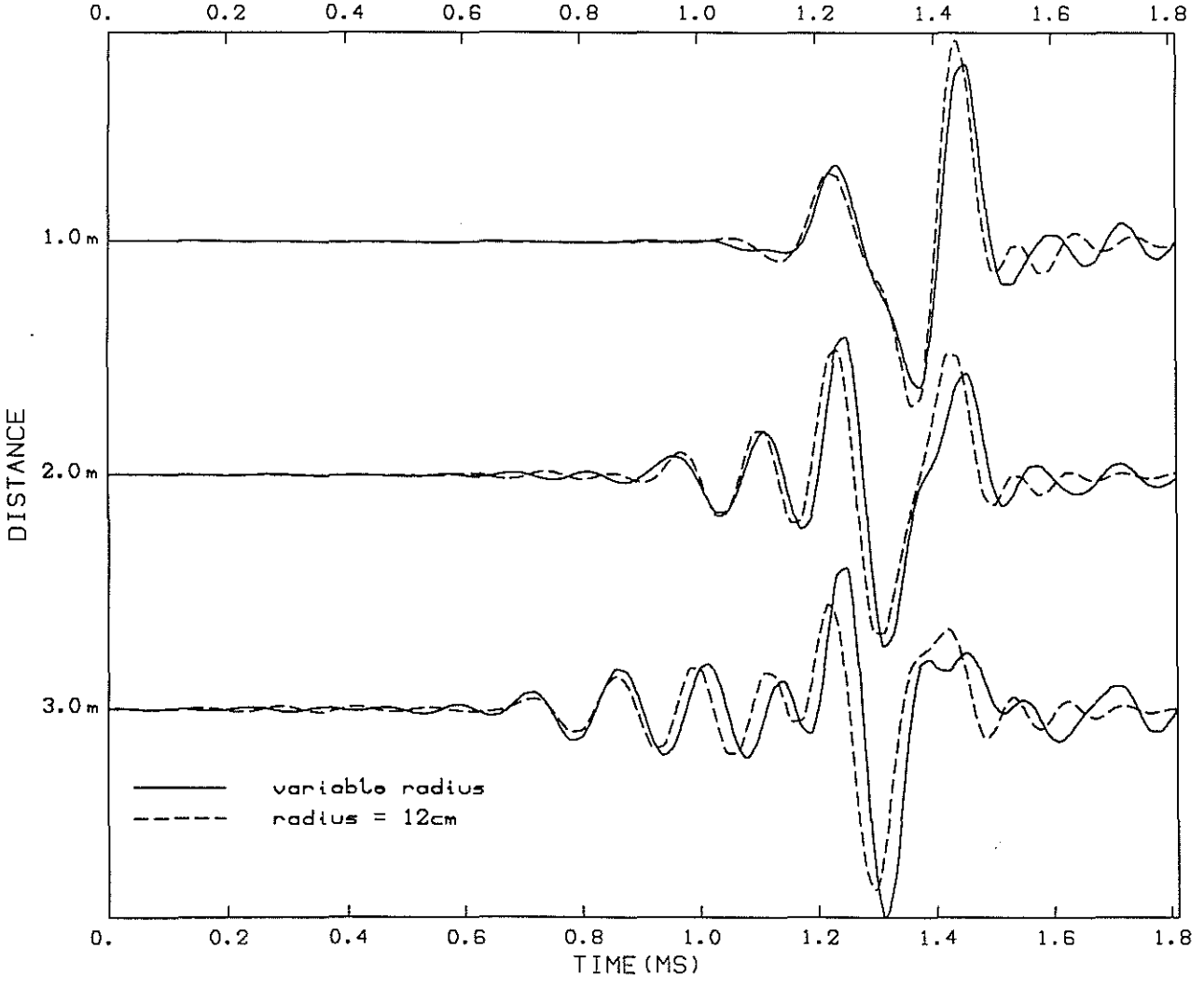

Figure 6: Comparison of the microseismograms obtained for the borehole geometry of Figure 1b with those that would be recorded for a borehole of constant radius equal to 12cm. The source is a Ricker pressure pulse of 4kHz peak frequency. The origin of the time scale is 1.4ms before the time of maximum pressure at the source minus a delay time which is equal to the axial distance divided by the tube wave velocity (1367m/s).

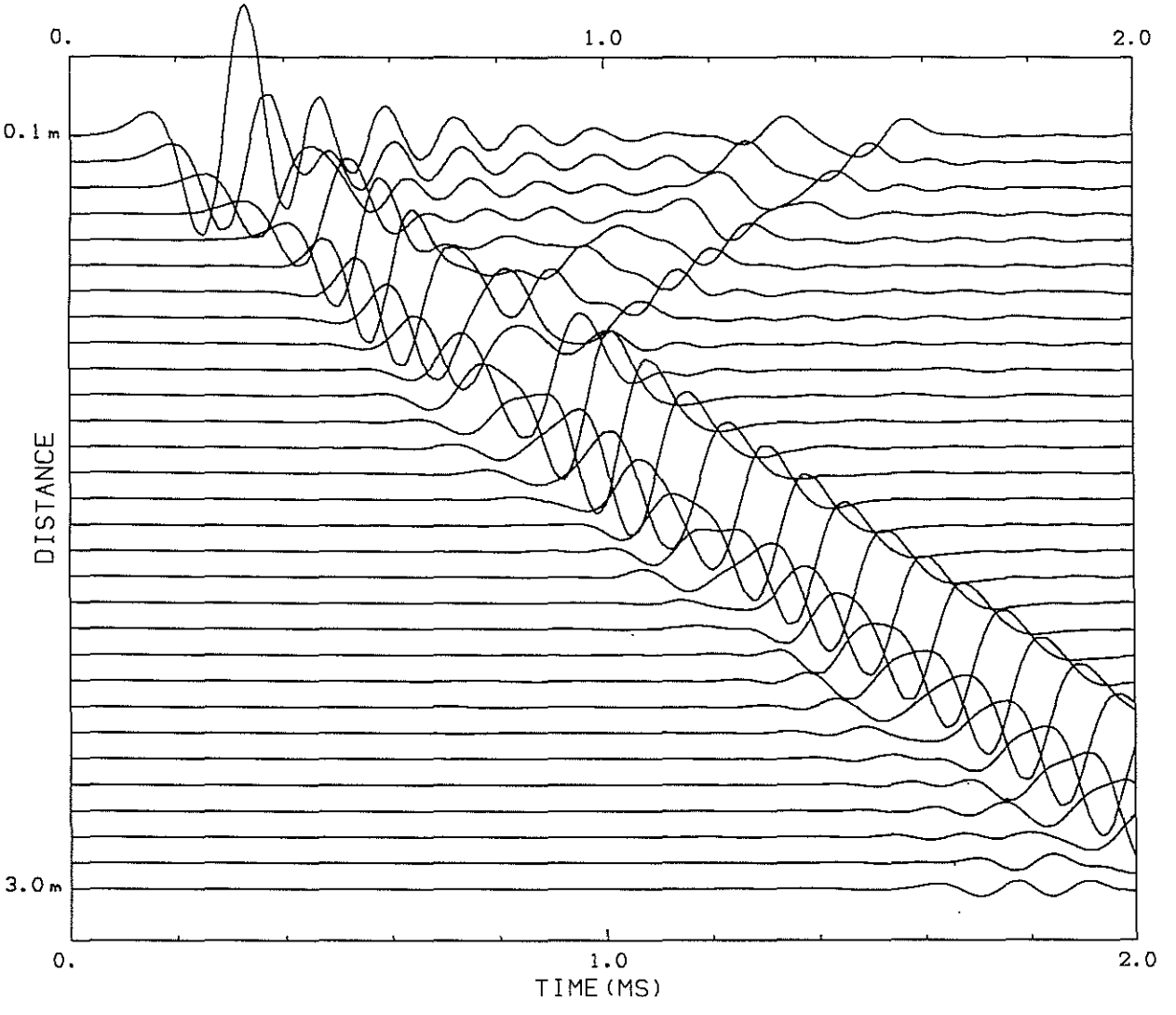

Figure 7: Synthetic acoustic logs obtained for the configuration of Figure 1c. The source is a Ricker pressure pulse of 3.5kHz peak frequency. The origin time is 0.15ms before the time of maximum pressure at the source.

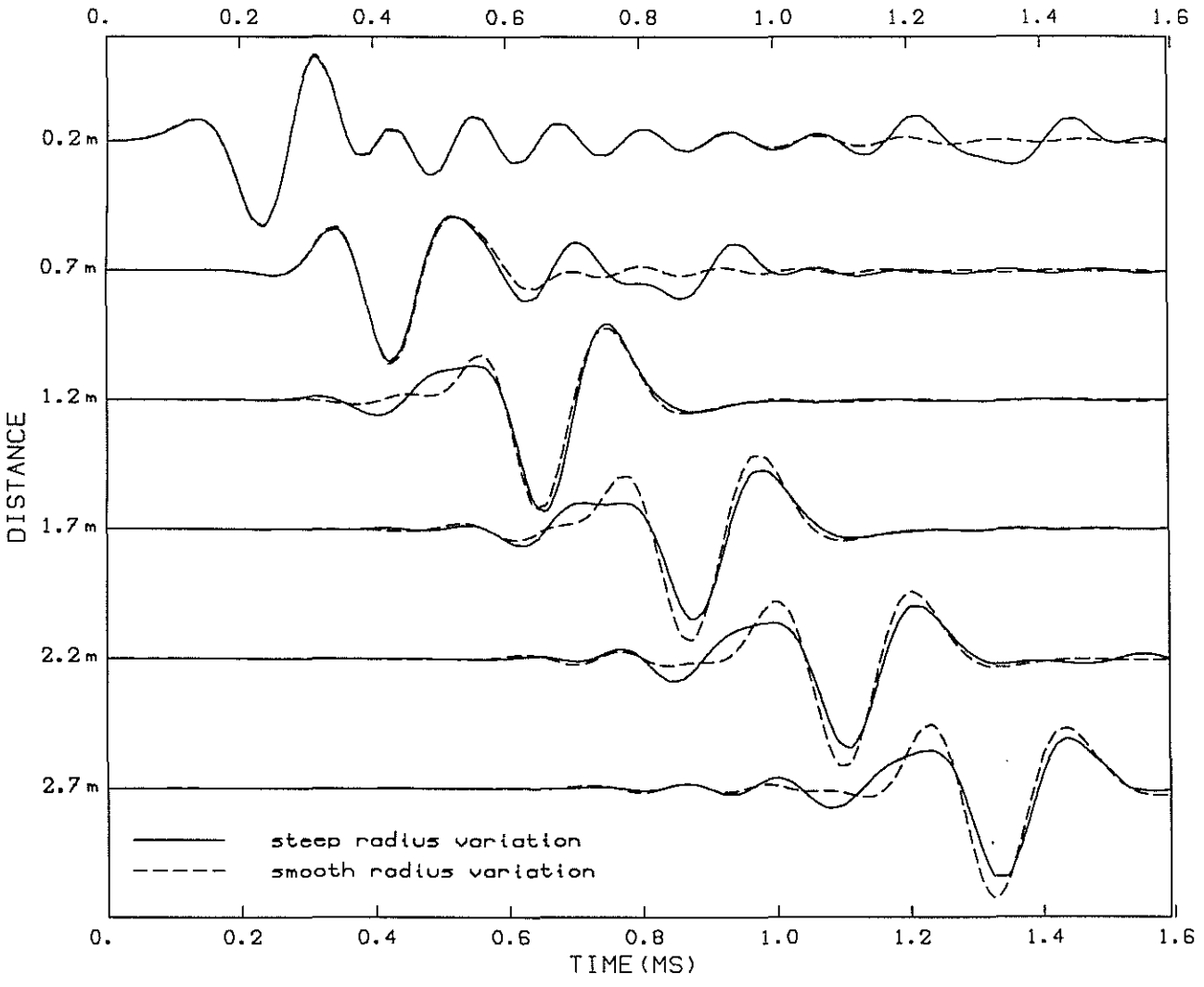

Figure 8: Comparison of the microseismograms obtained for the configurations of Figures 1a and 1b. The source is a Ricker pressure pulse of 3.5kHz peak frequency. The origin of the time scale is 0.15ms before the time of maximum pressure at the source minus a delay time which is equal to the axial distance divided by the P-wave velocity in the formation.